




Electron capture and emission dynamics of self-assembled quantum dots far from equilibrium with the environment

L. Schnorr , J. Labes , L. Kürten , and T. Heinzel *

Solid State Physics Laboratory, Heinrich-Heine-Universität Düsseldorf, 40204 Düsseldorf, Germany

C. Rothfuchs-Engels,[†] S. Scholz, A. Ludwig , and A. D. Wieck 

Lehrstuhl für Angewandte Festkörperphysik, Ruhr-Universität Bochum, 44780 Bochum, Germany



(Received 18 March 2021; revised 10 June 2021; accepted 6 July 2021; published 14 July 2021)

The electron transfer dynamics between self-assembled quantum dots and their environment are measured under nonequilibrium conditions by time-dependent capacitance spectroscopy. The quantum dots are embedded in a wide spacer, which inhibits elastic tunneling to or from the reservoirs. At certain bias voltages, electron capture and emission are both significant. A rate equation model is used to determine the corresponding transfer rates and the average occupation numbers of the dots as a function of the bias voltage.

DOI: [10.1103/PhysRevB.104.035303](https://doi.org/10.1103/PhysRevB.104.035303)

I. INTRODUCTION

Self-assembled quantum dots (SAQDs) [1] are not only studied extensively in fundamental science [2–5], they have also found their way into applications such as light-emitting diodes [6] or quantum dot lasers [7]. SAQDs are furthermore discussed in relation to transport devices, such as ultrasmall dynamic random access memory cells [8]. For this field, the dynamical properties of electronic transitions between the SAQD states and the environment are highly relevant. Many aspects of such charge transfers have been studied in the past two decades [9–23].

In standard elastic capacitance-voltage (CV) spectroscopy [9], resonances indicate the energetic alignment of the SAQD electron or hole states with the Fermi energy of the reservoir [9–12]. In this situation, the Fermi-Dirac distributions in the SAQD layer and in the back gate are identical, and we refer to this as *equilibrium*. The concept can also be extended to the nonequilibrium case [13,24]. In such CV experiments, the capture and emission times enter via the frequency dependence of the capacitance amplitudes and define an average, characteristic time constant [13,14]. However, the capture and emission time constants cannot be determined separately from such data. Recently, progress has been reported in this respect due to various experimental techniques. In transconductance spectroscopy, voltage pulses were used to prepare the charge state of the SAQDs, after which the capture and emission times were determined from the conductivity transients in a nearby two-dimensional electron gas [15,16]. Kurzman *et al.* [17] measured electron escape rates from SAQDs via the quenching of excitonic transitions. Also, electron tunneling rates have been determined by the effect of these electrons on the Auger ionization processes [18].

These techniques have in common that they rely on an electron reservoir close to the SAQD layer, i.e., with a distance of ≤ 30 nm, to allow elastic tunneling, or that spacer layers of larger thickness are sufficiently doped to enable a predominantly flat band between the reservoir and the SAQDs close to resonance [11]. Therefore, they are unsuitable to study capture rates of SAQDs embedded in large, weakly doped spacers to the reservoirs, as is common in optical applications such as light-emitting diodes [6], laser structures [7], single photon sources [2], or solar cells [25]. Recently, such highly isolated SAQDs were studied in relation to ultralong spin qubit lifetimes [26]. Some further experiments based on optical studies of electron filling processes in SAQDs [19–21] as well as indirect measurements studying the influence of the electron capture dynamics on the subsequent photon emission [22,23] have been carried out. Previous studies based on deep-level transient spectroscopy (DLTS) [27] have shown a significant influence of the electron capture dynamics on subsequent electron emission [28–31]. In these situations, the sample is out of equilibrium, but a local equilibrium can be reached after the transients have decayed. Hitherto, an all-electrical measurement scheme suited to directly study both the capture and emission transients of SAQD layers with large distances to the reservoirs and/or out of equilibrium has not been reported yet.

Here, we show that such a scheme can be implemented based on established DLTS measurement techniques by measuring both capture and emission transients. For this proof of principle, an SAQD layer is embedded into an insulating layer providing distances of ≈ 500 nm from the electron reservoirs. In a significant bias voltage interval, capture and emission occurs simultaneously, resulting in nontrivial capacitance transients. We analyze them with a rate equation model to obtain the voltage-dependent capture and emission rates as well as the steady-state occupation probability of the dots. In Sec. II, the sample design and the experimental setup are described. The experimental results are reported in Sec. III. The measurements are interpreted within a rate equation model in Sec. IV. The paper concludes with a summary and an outlook (Sec. V).

*Thomas.Heinzel@hhu.de

[†]Present address: DESY, Notkestrasse 85, 22607 Hamburg, Germany.

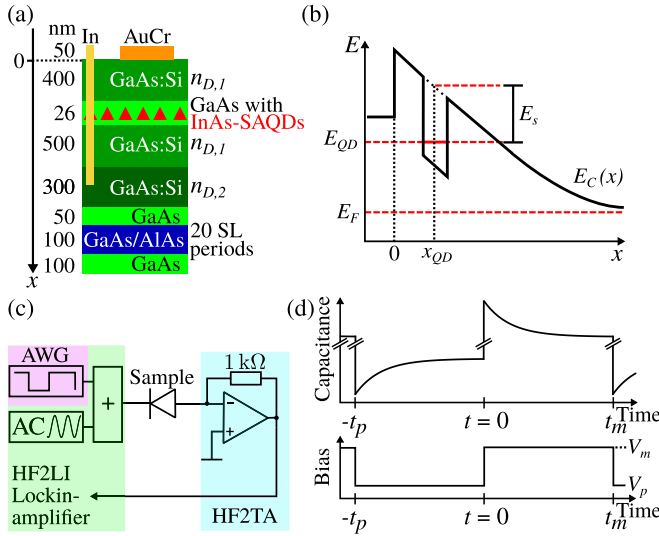


FIG. 1. (a) Cross-sectional schematic view of the sample layout. The SAQD layer is indicated by the red triangles. (b) Schematic band diagram for the case of a negative voltage applied to the top gate with respect to the grounded embedded electrode, including our conventions for the quantities of relevance. (c) Scheme of the measurement setup. (d) Illustration of the bias voltage pulses and transient capacitive response.

II. SAMPLE CHARACTERIZATION AND EXPERIMENTAL TECHNIQUES

In the structures under study, the SAQDs reside in a plane inside a semiconductor heterostructure grown by molecular beam epitaxy. On top of a GaAs single crystal, a GaAs/AlAs short-period superlattice is grown that decreases the surface roughness and acts as a protective barrier for impurities that may segregate from the substrate toward the SAQD layer; see Fig. 1(a). An embedded electrode is formed by a 300 nm layer of highly Si-doped GaAs with a doping density of $n_{D,2} = 2 \times 10^{18} \text{ cm}^{-3}$. A weakly Si-doped GaAs spacer layer (doping density $n_{D,1} = 2 \times 10^{16} \text{ cm}^{-3}$) establishes a large distance between this electrode and the SAQD layer, which is grown in the Stranski-Krastanov mode. The layer contains InAs SAQDs with a sheet density of 10^{11} cm^{-2} and is surrounded by in total 26 nm of undoped GaAs. The SAQDs have a nearly circular base of $\approx 30 \text{ nm}$ diameter, and a height of approximately 7 nm. A weakly doped GaAs layer (thickness 400 nm, doping density $n_{D,1} = 2 \times 10^{16} \text{ cm}^{-3}$) covers the SAQDs and forms the surface of the heterostructure.

The wafer is cut into pieces with an area of $5 \text{ mm} \times 5 \text{ mm}$. Optical lithography and subsequent metallization are applied to define a Cr/Au top electrode of lateral size $0.3 \text{ mm} \times 0.3 \text{ mm}$, and, via a subsequent alloy step, an indium Ohmic contact to the back electrode. In terms of DLTS, the overall structure can be regarded as a Schottky diode, with the SAQD layer representing an ensemble of defect states. This structure is the same as that used in Ref. [32].

The sample is inserted into a liquid nitrogen dewar. At a temperature of $T = 77 \text{ K}$, negative DC bias voltages are applied to the top gate with respect to the back contact, which is kept at the virtual ground of an HF2TA transimpedance

amplifier ($Z = 1 \text{ k}\Omega$) from Zurich Instruments. The voltage pulses are generated using a Keithley Model 3390 arbitrary waveform generator (AWG) with a transition time of 100 ns.

The potential energy of the electrons increases as one approaches the top gate from the back contact; see Fig. 1(b) for a sketch of the potential landscape, where also the labeling conventions of the energies and distances with relevance for the following discussions are introduced. The electronic ground-state energy of the SAQDs is denoted by E_{QD} , while the corresponding binding energy E_s is the energy difference $E_C(x_{QD}) - E_{QD}$, with $x_{QD} = 413 \text{ nm}$ being the distance of the SAQD layer from the sample surface. E_F denotes the Fermi energy for electrons in the back contact. For the measurements of capacitance transients, an AC voltage of 20 mV amplitude and a frequency of 28.9 MHz is superimposed to the DC bias voltages, and the out-of-phase signal of the resulting current is measured as a function of time (corresponding to transient capacitance) using an HF2LI lock-in amplifier from Zurich Instruments and sampled using a PicoScope 5444B digital oscilloscope from Pico Technology. All transients were sampled with a time resolution of at least $\Delta t = 10 \mu\text{s}$ over a variable recording time. This measurement configuration is illustrated in Fig. 1(c). By applying different bias voltages to the gate [Fig. 1(d)], the energies of the electronic states in the SAQDs can be tuned, and the system reacts by electron capture or emission, respectively, the time dependence of which can be monitored by capacitance transients. A certain initial condition is established by applying a preparation voltage V_p for a time t_p . Afterwards, a measurement voltage V_m is applied for a time t_m during which the capacitance transient $C(t)$ is recorded.

III. EXPERIMENTAL RESULTS

We first look at the electron filling dynamics as a function of V_m by Laplace-DLTS (LDLTS) [33].

The capture transients are measured after applying a preparation voltage $V_p = -2.0 \text{ V}$ for $t_p = 50 \text{ ms}$ to ensure that the emission processes have decayed well below the detection threshold [32]. Hence, the SAQDs can be expected to be empty to a good approximation. For each V_m , the capacitance transients are averaged over 3×10^5 individual traces in order to obtain a signal-to-noise level > 1000 as required for a numerically stable inverse Laplace transform.

In Fig. 2(a), typical averaged capacitance transients observed for the electron capture are reproduced. Already in the raw data, a strong dependence of the characteristic decay time τ on V_m is observed. As V_m is increased, τ decreases. In previous isothermal measurements of the emission rates as a function of the bias voltage [32], we observed very good agreement with the Vincent theory of thermally assisted tunneling [34], where the voltage dependence enters via the transparency of an approximately triangular barrier. Thus, as a first assumption, it appears plausible to apply this theory to the voltage dependence of the capture rate as well. According to the Fowler-Nordheim picture [35], the transparency η of this tunnel barrier is given by

$$\eta = \exp\left(-\frac{4}{3} \frac{\sqrt{2m^*} E_s^{3/2}}{q\hbar F}\right), \quad (1)$$

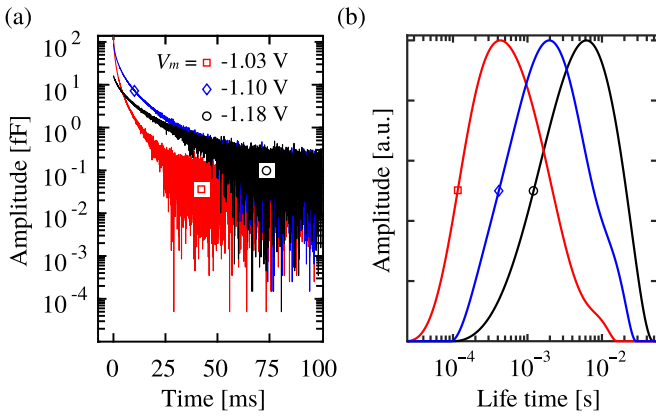


FIG. 2. Absolute value of the capacitance transients for three different measurement voltages V_m after depletion of the SAQDs by a preparation voltage of $V_p = -2.0$ V (a) and the corresponding Laplace spectra, with normalized amplitudes (b).

where F is the electric field and m^* is the effective electron mass. Since band-structure calculations show an approximately linear relationship between V_m and F [36], and an increase in η leads to an increased charge-transfer rate, one expects an increasing time constant as V_m is increased, in striking contrast to the observations. We note that this ansatz does not imply that the captured electrons originate from the back electrode; see below.

This indicates that for the capture dynamics in our system, elastic tunneling across the barrier between the SAQDs and the conduction band is of marginal relevance. Rather, since an increase of V_m decreases $E_{\text{QD}} - E_F$, this observation suggests that the capture of electrons has a thermally activated character.

The most obvious assumption is thermal activation across the energy barrier $E_a = E_C(x_{\text{QD}}) - E_F$ between the back contact and the quantum dots; see Fig. 1(b). An equilibrium model for this process, however, leads to a contradiction with the measurements. To see this, we have calculated the band structure for the applied bias voltage to obtain $E_C(x, V)$ and the local electron density $n_e(x, V)$ at 77 K, using a one-dimensional Poisson-Schrödinger solver [37] and GNU-Octave [38]. In detail, the SAQD layer is not included in the simulation but rather is included by hand afterwards. This is possible since the energies of the SAQD states with respect to the GaAs band edge are well known from many experiments (see, e.g., Refs. [22,39]), and in particular also for our present system from capacitance transients for the emission process reported earlier [32]. The sample structure was simulated as given in Fig. 1(a) with a built-in potential of 0.63 V as obtained from a conventional $C^{-2}(V)$ analysis [36]. If we assume a Fermi-Dirac distribution of the electrons in the back contact, the occupation probability for electrons at the energy levels of the SAQDs is merely 10^{-26} at $V_m = -1$ V, where a strong charging signal can be observed. Furthermore, integrating the calculated local electron density over an interval of ± 100 nm around the SAQD layer and multiplying it with the gate area yields an average number of only 10^{-12} electrons available per dot. Thus, electron capture of electrons from the back contact within an equilibrium picture can safely be

excluded for the pulse voltages used here. This is also in tune with our observation of a significant DC current flow between the top electrode and the back gate under the bias voltages used here [36]. In the following, we therefore do not assume an equilibrium distribution for the electrons between the SAQDs and the back gate [24], although it is not generally excluded and may be possible for specific bias voltages. Instead, we describe the transfer process empirically in terms of capture and emission rates without any reference to the conduction band profile.

The inverse Laplace transforms of the transients give the corresponding lifetime distributions; see Fig. 2(b). Each transient is dominated by a single time constant, in contrast to previous measurements of electron emission on the same sample, where separate time constants from the single- and two-electron state could be observed [32]. It should be emphasized that the peak shape originates from the regularization method necessary to stabilize the numerical Laplace inversion, and it cannot be interpreted in terms of physical sample properties.

The amplitudes of the transients drop rapidly as V_m is decreased below -1.0 V, i.e., a decrease by an order of magnitude is found as V_m is decreased from -1.03 to -1.18 V. This strong suppression puts a lower limit to the accessible range of V_m where capture can be observed.

To study the voltage dependence of the charge-transfer dynamics, we have performed lock-in DLTS [40] measurements at $T = 77$ K using a square-wave voltage pulse with $t_p = t_m = 94.9$ ms, and a transition time of $t_{p \leftrightarrow m} = 100$ ns, as sketched in Fig. 1(d). The voltages V_p and V_m cover all combinations within $[-3.0$ V, 0 V] with a step size of $\Delta V = 40$ mV. After applying V_p for t_p , the transient is measured at V_m applied for the time interval t_m with a time resolution of $\Delta t = 10$ μ s. Prior to the start of each averaging process, we wait for a settling time of 3 s in order to let the system adjust to the new parameters. After measuring 500 identical transients per combination of V_p and V_m , the lock-in signal $S(V_p, V_m)$ is calculated [40] from the average of these transients, where

$$S(V_p, V_m) = \sum_{i=1}^{N_t/2} C(t_i, V_p, V_m) - \sum_{i=N_t/2+1}^{N_t} C(t_i, V_p, V_m), \quad (2)$$

with the total number of data points N_t in the transient. No gate-off period has been used, since ringing/overshooting of our setup was negligible for the parameter ranges in use. The lock-in method is used here since it is impossible to acquire the required large amount of data by LDLTS in a reasonable time. The results are shown in Fig. 3(a). A positive signal (orange to dark red) corresponds to an increase in charge stored at the SAQD layer, while a negative one (dark blue to yellow) indicates a decrease. A vanishing signal represents either no charge transfer or a transfer that is too fast or too slow to cause a significant change during t_m .

Two prominent features can be observed. For $V_p \lesssim -1$ V and $V_m \in [-1.2, -1.0]$ V the positive signal shows that electron capture dominates, at a rate within the rate window of the lock-in function. Likewise, for $V_p \gtrsim -1$ V and $V_m \in [-2.0, -1.0]$ V the signal is negative, indicative of predominant electron emission. While both of these features depend strongly on V_m , there is almost no dependence on the

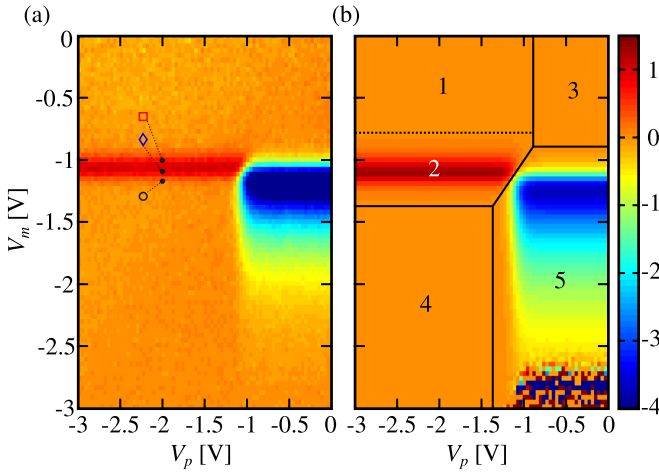


FIG. 3. Color plot of the measured (a) and calculated (b) lock-in signal $S(V_p, V_m)$ in arbitrary units as a function of V_p and V_m . The same color map applies to both subfigures. The black dots in (a) mark the points where the three capture transients shown in Fig. 2 (with the corresponding symbols) were taken. The numbers in (b) denote different charge-transfer regimes as explained in the text.

preparation voltage outside of the transition interval, given by $V_p \approx (-1.0 \pm 0.2)$ V. As we will show in more detail below, the capture and emission rates are comparable in this interval, and the average occupation probability of the relevant SAQD states varies around 50%. Kapteyn *et al.* [29] studied the dependence of the emission DLTS signal amplitude both as a function of V_p for a fixed V_m and as a function of V_m for a fixed V_p . Their approach is equivalent to lineouts of the region $V_p > V_m$ of our Fig. 3, since in the work of Kapteyn *et al.* only the electron emission was measured. Qualitatively, their data match our findings very well. Here, we study the capture dynamics over a wide parameter range, leading to information from both the dynamics and magnitudes of the filling process, as well as from its interplay with the subsequent emission.

IV. RATE EQUATION MODEL AND INTERPRETATION

Since we study the SAQD system in a nonequilibrium state, an interpretation of the data based on a self-consistent solution of the Poisson-Schrödinger equation [37], which corresponds to a band structure in equilibrium, is inadequate here, while a calculation of the nonequilibrium band structure is beyond our scope. Rather, we proceed by interpreting the experiments in terms of a rate equation model. This approach does not depend on geometric properties or the material compositions of the SAQDs. The emission rates from the one- and two-electron state can be measured separately by LDLTS [32]. On the other hand, the capture dynamics reported above show only one time constant. We thus model our system by assuming that an SAQD can be charged with up to two electrons. Capture occurs with a voltage-dependent rate $c(V)$ that is independent of the charge state of the dot. We assume two separate rates $r_{10}(V)$ and $r_{21}(V)$ for emission from the one- and the two-electron state, respectively, and a capture rate independent of the charging state. Further studies at lower temperatures may be able to resolve the state-dependence of

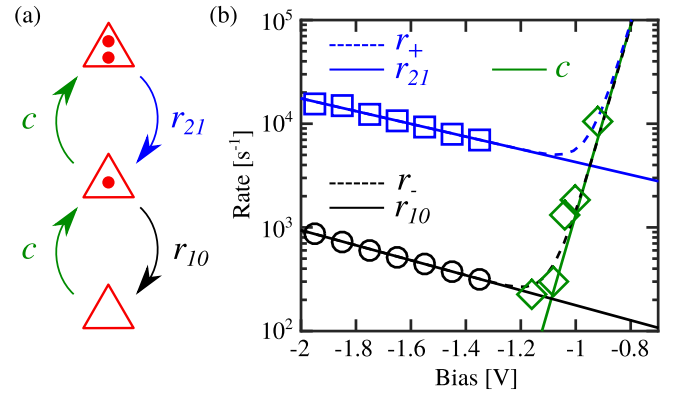


FIG. 4. (a) Illustration of the rate equation model, Eqs. (3)–(5). Red triangles denote SAQDs and the full red circles show electrons therein, while the transfer rates are symbolized by arrows. (b) Measured transfer rates in comparison to the rate equation model. The symbols denote isothermal rate constant measurements of the two emission paths [32] and of the capture process, respectively. The solid lines show the transfer rates according to Eqs. (8)–(10), using the results of the fit described in the text. The dashed lines represent the rate constants according to Eq. (7).

the capture rate, an experiment that is beyond our scope here. The electron transfer dynamics can be described by the set of differential equations for the time evolution of the density of SAQDs that have either captured zero, one, or two electrons:

$$\dot{n}_0 = -cn_0 + r_{10}n_1, \quad (3)$$

$$\dot{n}_1 = -cn_1 + r_{21}n_2 + cn_0 - r_{10}n_1, \quad (4)$$

$$\dot{n}_2 = +cn_1 - r_{21}n_2. \quad (5)$$

Here, a dotted symbol denotes the time derivative of the quantity. The relations of the quantities in this model are illustrated in Fig. 4(a). From its solution, the total charge density in the SAQD layer $n(t)$ can be derived, which is proportional to the measured capacitance transients,

$$C(t) \propto n(t) = n_1(t) + 2n_2(t). \quad (6)$$

Equations (3)–(5) were solved analytically using the SymPy library [41], and the solutions are given in the supplemental material [36]. By analyzing the resulting expression for $C(t)$ [Eq. (6)], it can be shown that it is a superposition of two exponential decays with two observable charge-transfer rates r_{\pm} given by

$$r_{\pm} = \frac{1}{2}(2c + r_{10} + r_{21} \pm \sqrt{4cr_{10} + r_{10}^2 - 2r_{21}r_{10} + r_{21}^2}). \quad (7)$$

This analytical solution is well-known from the study of multistep reaction kinetics in chemistry where this set of differential equations describes the time-dependent concentration of the substances involved [42]. Here, we use this solution for a wide variety of initial conditions, as opposed to its use in chemistry, where the equations are often simplified due to a specific initial condition.

TABLE I. Fit parameters used to calculate the results shown in Figs. 3(b) and 4(b).

m_{10} (V ⁻¹)	n_{10}	m_{21} (V ⁻¹)	n_{21}	m_c (V ⁻¹)	n_c
-1.67	3.51	-1.41	6.94	21.02	28.21

Based on previous measurements of an exponential voltage dependence of the emission rates [32], we model the rates as follows:

$$r_{10}(V) = \exp(m_{10}V + n_{10}) s^{-1}, \quad (8)$$

$$r_{21}(V) = \exp(m_{21}V + n_{21}) s^{-1}, \quad (9)$$

$$c(V) = \exp(m_c V + n_c) s^{-1}. \quad (10)$$

The constants introduced here— m_{ij} , n_{ij} , m_c , and n_c —are to be determined by a fit to the measured data. For the emission rates, the m_{ij} correspond to the slope of the approximated Vincent correction factor [43], whereas the n_{ij} represents the logarithm of the pure thermal emission rates without any residual voltage dependence. Due to the lack of equivalent theories for the capture process that we are aware of, the interpretation of the respective fit parameters remains to be discussed. To calculate the capacitance transients for any combination of V_p and V_m , we need to insert into Eqs. (8)–(10) the exact time dependence of the bias transition between V_p and V_m and assume plausible initial conditions for $n_i(t = 0)$.

The time constants of the transients vary greatly as a function of the bias voltage and can assume quite high values. To reach the steady state as the initial condition for each measurement would require an adaptation of t_p for each V_p and take an *a priori* unknown amount of time. Fortunately, the model does not require a steady state as the initial condition, which greatly simplifies the measurement process. We assume that after t_p , a steady state has not necessarily been reached, and we take into account the exact time evolution of the preparation transients as a function of V_p . This evolution depends in turn on the time evolution of the previous measurement. This is taken into account by solving Eqs. (3)–(5) for an arbitrary initial condition, for example $n_0(t = 0) = 1$ and $n_1(t = 0) = n_2(t = 0) = 0$, over five subsequent pulse cycles. We observe that after already three cycles, the signal is independent of the selected initial condition. Therefore, we accept the final transient for V_m as the solution.

To obtain the unknown parameters in Eqs. (8)–(10), we fit our model to the measurements shown in Fig. 3(a). Figure 3(b) shows the lock-in signal obtained from the calculated transients using the same time resolution as in the measurement. In addition to the parameters in Eqs. (8)–(10), a scaling factor was fitted to account for the unknown proportionality in Eq. (6). The artifacts for $V_m < -2.5$ V are due to limited floating point accuracy while calculating Eqs. (8) and (9), and they were excluded from the fit. The relevant fitting parameters are given in Table I.

We note that the values for m_{10} and m_{21} agree well with the voltage dependence of the Vincent correction factor used in previous discussions of the isothermal emission rates from the *s*-states in Ref. [32]: The correction factor [36] shows a voltage dependence that can be approximated to a very good

degree by Eqs. (8) and (9). For both *s*-states, such an approximation for $V_m < -1.0$ V, under which the emission features were observed, yields a slope of $m = -1.59$ V⁻¹, i.e., the Vincent correction factor depends only weakly on the binding energy. We attribute the remaining, charge-state-dependent variations of our empirical model to the larger bias voltage range studied here, and possibly to additional interactions not accounted for in the Vincent theory. Additionally, the voltage-independent emission rates given by $\exp(n_{ij})$ closely match those obtained after applying the Vincent correction; see Fig. 4(b) in Ref. [32]. The capture constants m_c and n_c , finally, parametrize the voltage dependence of the capture rate, the physical interpretation of which is, to the best of our knowledge, unclear due to a lack of established theories.

Good agreement between the measurement and the model is observed. Figure 4(b) shows the resulting voltage dependence of the rates [Eqs. (8)–(10)] as solid lines. The symbols represent LD LTS measurements of the emission rates [32] and the capture rates shown in Sec. III, respectively, while the dashed lines show the charge-transfer rates according to Eq. (7). In the voltage interval where the emission rates could be measured by LD LTS, the observable charge-transfer rates are identical to the respective emission rates, indicating that here, electron capture is negligible. On the other hand, the LD LTS capture measurements reported above have been carried out at voltages where the charge-transfer rates have not yet converged to $c(V)$. Rather, they are influenced by competing emission processes in a non-negligible way. It should be noted, therefore, that great care is required when transients measured in such a regime are related to a band-structure profile. From the smallest observable charge-transfer rate of $r_- \approx 2.5 \times 10^2$ s⁻¹ at $V \approx -1.2$ V we can calculate that one has to wait at this bias voltage for at least 19 ms until the corresponding transients have decayed by 99%. This corresponds to the worst case of the time required for a saturated charging pulse. Even though in our measurement this time was exceeded for all measurements, a saturated pulse did not generally lead to an equilibrium distribution. After a decayed transient, the SAQDs are merely in a steady-state configuration that appears to be independent of the charge distribution in the rest of the sample.

We proceed by extracting this steady-state configuration of the SAQDs as a function of the bias voltage, characterized by their average occupancy with electrons. This configuration corresponds to the solution of Eqs. (3)–(6) in the limit $t \rightarrow \infty$. The results are shown in Fig. 5.

For $V \lesssim -1.2$ V, the dots are empty in the stationary state, while they are occupied with two electrons for $V \gtrsim -0.85$ V. In the transition region in Figs. 3 and 4(b), the occupancy changes from 0 to 2 as V is increased, with a maximum for n_1 at $V = -1.025$ V. This is in tune with the observed strong decrease of the transient amplitude as the bias voltage decreases below -1.1 V (see Fig. 2). Furthermore, it confirms assumptions made previously, namely that the dots can be prepared in an empty state at $V_p \leq -1.4$ V and in a filled state at $V_p \geq -0.5$ V. Moreover, a physical interpretation of the different areas observed in Fig. 3 is now straightforward: In Region 1, the SAQDs get emptied during V_p and capture electrons at a fast rate above the resolution threshold during V_m . In Region 2, the capture rate falls inside the measurable

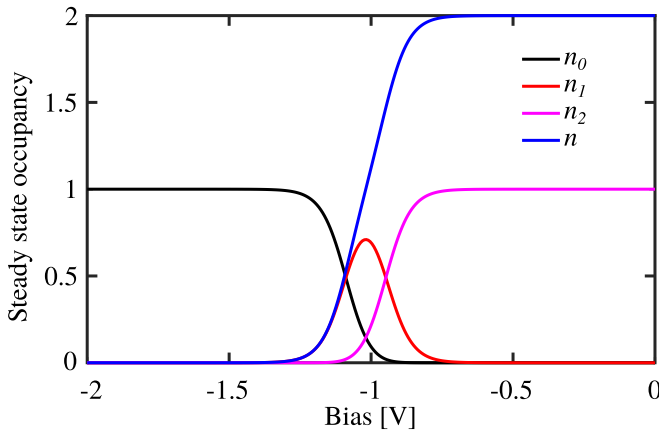


FIG. 5. Steady-state occupancy of the zero-, one-, and two-electron configurations $n_i(V)$ and the average number of electrons per dot $n(V)$.

window, while in Region 4, electron capture is negligible during t_m , i.e., the SAQDs are essentially empty. We note that only in this region is the observed electron occupation of the dots in equilibrium with the back contact. In Region 3, on the other hand, the SAQDs are filled with (at least) two electrons during V_p and remain charged during V_m . As V_m decreases, one enters into Region 5, where electron emission can be observed down to voltages of approximately -2 V. At even lower voltages, the emission becomes too fast to be monitored with our setup.

V. SUMMARY AND OUTLOOK

The reported experiments demonstrate that it is possible to determine the electron capture and emission rates of SAQDs by transient capacitance spectroscopy far from equilibrium

and without knowledge regarding the band-structure profile under these conditions. A system of coupled rate equations enables the extraction of the rate constants for electron capture and emission from the observed transients, which are influenced by both processes in the intermediate regime, where capture and emission occur simultaneously. Furthermore, by this analysis, the average occupation number of the dots with electrons as well as the voltage ranges for exclusively filling or emptying the dot states are obtained. Moreover, the concepts developed here are conceptually applicable to a variety of SAQD material systems as well as to hole states, in particular for samples where the SAQD layer is far away from electron reservoirs, like in laser structures or light-emitting diodes. Further studies on the present system may comprise isothermal measurements at various temperatures in order to determine the temperature dependence of the transfer rates, as well as possible influences of defects in the environment of the SAQD layer [44]. Advances regarding the sample inhomogeneity or by faster electronics, as well as measurements at lower temperatures, may enable the determination of state-dependent capture and emission rates. A better understanding of the transfer processes may be possible with the help of self-consistent simulations of the band structure out of equilibrium.

ACKNOWLEDGMENTS

Computational support and infrastructure was provided by the Centre for Information and Media Technology (ZIM) at the University of Düsseldorf (Germany). C.R.-E., S.S., A.D.W., and A.L. gratefully acknowledge support of TRR 160/2-Project B04, DFG 383065199, and the DFH/UFA CDFA-05-06.

-
- [1] D. Leonard, M. Krishnamurthy, C. M. Reaves, S. P. Denbaars, and P. M. Petroff, *Appl. Phys. Lett.* **63**, 3203 (1993).
 - [2] P. Michler, A. Kiraz, C. Becher, W. V. Schoenfeld, P. M. Petroff, L. Zhang, E. Hu, and A. Imamoglu, *Science* **290**, 2282 (2000).
 - [3] M. Kroutvar, Y. Ducommun, D. Heiss, M. Bichler, D. Schuh, G. Abstreiter, and J. J. Finley, *Nature (London)* **432**, 81 (2004).
 - [4] C. L. Salter, R. M. Stevenson, I. Farrer, C. Nicoll, D. A. Ritchie, and A. J. Shields, *Nature (London)* **465**, 594 (2010).
 - [5] A. Faraon, A. Majumdar, D. Englund, E. Kim, M. Bajcsy, and J. Vuckovic, *New J. Phys.* **13**, 055025 (2011).
 - [6] I. L. Krestnikov, N. A. Maleev, A. V. Sakharov, A. R. Kovsh, A. E. Zhukov, A. F. Tsatsulnikov, V. M. Ustinov, Z. I. Alferov, N. N. Ledentsov, D. Bimberg, and J. A. Lott, *Semicond. Sci. Technol.* **16**, 844 (2001).
 - [7] V. M. Ustinov, N. A. Maleev, A. E. Zhukov, A. R. Kovsh, A. Y. Egorov, A. V. Lunev, B. V. Volovik, I. L. Krestnikov, Y. G. Musikhin, N. A. Bert, P. S. Kopev, and Z. I. Alferov, *Appl. Phys. Lett.* **74**, 2815 (1999).
 - [8] A. Marent, T. Nowozin, J. Gelze, F. Luckert, and D. Bimberg, *Appl. Phys. Lett.* **95**, 242114 (2009).
 - [9] H. Drexler, D. Leonard, W. Hansen, J. P. Kotthaus, and P. M. Petroff, *Phys. Rev. Lett.* **73**, 2252 (1994).
 - [10] O. Wibbelhoff, A. Lorke, D. Reuter, and A. W. Wieck, *Appl. Phys. Lett.* **86**, 092104 (2005).
 - [11] P. N. Brounkov, A. Polimeni, S. T. Stoddart, M. Henini, L. Eaves, P. C. Main, A. R. Kovsh, Y. G. Musikhin, and S. G. Konnikov, *Appl. Phys. Lett.* **73**, 1092 (1998).
 - [12] P. Kailuweit, D. Reuter, A. Wieck, O. Wibbelhoff, A. Lorke, U. Zeitler, and J. Maan, *Physica E* **32**, 159 (2006).
 - [13] S. R. Valentin, J. Schwinger, P. Eickelmann, P. A. Labud, A. D. Wieck, B. Sothmann, and A. Ludwig, *Phys. Rev. B* **97**, 045416 (2018).
 - [14] R. J. Luyken, A. Lorke, A. O. Govorov, J. P. Kotthaus, G. Medeiros-Ribeiro, and P. Petroff, *Appl. Phys. Lett.* **74**, 2486 (1999).
 - [15] A. Beckel, A. Ludwig, A. D. Wieck, A. Lorke, and M. Geller, *Phys. Rev. B* **89**, 155430 (2014).
 - [16] D. Zhou, A. Beckel, A. Ludwig, A. D. Wieck, A. Lorke, and M. Geller, *Appl. Phys. Lett.* **106**, 243105 (2015).
 - [17] A. Kurzman, A. Ludwig, A. D. Wieck, A. Lorke, and M. Geller, *Appl. Phys. Lett.* **108**, 263108 (2016).

- [18] A. Kurzmann, A. Ludwig, A. D. Wieck, A. Lorke, and M. Geller, *Nano Lett.* **16**, 3367 (2016).
- [19] S. Raymond, S. Fafard, P. J. Poole, A. Wojs, P. Hawrylak, S. Charbonneau, D. Leonard, R. Leon, P. M. Petroff, and J. L. Merz, *Phys. Rev. B* **54**, 11548 (1996).
- [20] P. Miska, J. Even, O. Dehaese, and X. Marie, *Appl. Phys. Lett.* **92**, 191103 (2008).
- [21] Y. I. Mazur, V. G. Dorogan, E. Marega, Z. Y. Zhuchenko, M. E. Ware, M. Benamara, G. G. Tarasov, P. Vasa, C. Lienau, and G. J. Salamo, *J. Appl. Phys.* **108**, 074316 (2010).
- [22] A. Schramm, S. Schulz, J. Schaefer, T. Zander, C. Heyn, and W. Hansen, *Appl. Phys. Lett.* **88**, 213107 (2006).
- [23] A. Walther, J. Bollmann, H. Kissel, H. Kirmse, W. Neumann, and W. Masselink, *Phys. B* **273-274**, 971 (1999).
- [24] M. Geller, *Appl. Phys. Rev.* **6**, 031306 (2019).
- [25] A. Luque, A. Marti, and C. Stanley, *Nat. Photon.* **6**, 146 (2012).
- [26] G. Gillard, I. Griffiths, G. Ragunathan, A. Ulhaq, C. McEwan, E. Clarke, and E. A. Chekhovich, *npj Quantum Inf.* **7**, 43 (2021).
- [27] D. V. Lang, *J. Appl. Phys.* **45**, 3023 (1974).
- [28] S. Anand, N. Carlsson, M.-E. Pistol, L. Samuelson, and W. Seiffert, *Appl. Phys. Lett.* **67**, 3016 (1995).
- [29] C. M. A. Kapteyn, F. Heinrichsdorff, O. Stier, R. Heitz, M. Grundmann, N. D. Zakharov, D. Bimberg, and P. Werner, *Phys. Rev. B* **60**, 14265 (1999).
- [30] S. Schulz, A. Schramm, C. Heyn, and W. Hansen, *Phys. Rev. B* **74**, 033311 (2006).
- [31] O. Engström, M. Kaniewska, M. Kaczmarczyk, and W. Jung, *Appl. Phys. Lett.* **91**, 133117 (2007).
- [32] L. Schnorr, T. Heinzl, S. Scholz, A. Ludwig, and A. D. Wieck, *J. Appl. Phys.* **124**, 104301 (2018).
- [33] L. Dobaczewski, P. Kaczor, I. D. Hawkins, and A. R. Peaker, *J. Appl. Phys.* **76**, 194 (1994).
- [34] G. Vincent, Ph.D. thesis, Université de Claude Bernard Lyon, Institut National des Sciences Appliquées, 1978.
- [35] R. H. Fowler and L. Nordheim, *Proc. Roy. Soc. Lond. A* **119**, 173 (1928).
- [36] See Supplemental Material at <http://link.aps.org/supplemental/10.1103/PhysRevB.104.035303> for details.
- [37] G. Snider, 1D Poisson, <https://www3.nd.edu/~gsnider/>, Accessed on Jun 9th, 2021.
- [38] J. W. Eaton, D. Bateman, S. Hauberg, and R. Wehbring, GNU Octave version 5.2.0 manual: a high-level interactive language for numerical computations, <https://octave.org/doc/v5.2.0/>, 2020.
- [39] S. Schulz, S. Schnüll, C. Heyn, and W. Hansen, *Phys. Rev. B* **69**, 195317 (2004).
- [40] D. S. Day, M. Y. Tsai, B. G. Streetman, and D. V. Lang, *J. Appl. Phys.* **50**, 5093 (1979).
- [41] A. Meurer, C. P. Smith, M. Paprocki, O. Čertík, S. B. Kirpichev, M. Rocklin, A. Kumar, S. Ivanov, J. K. Moore, S. Singh, T. Rathnayake, S. Vig, B. E. Granger, R. P. Muller, F. Bonazzi, H. Gupta, S. Vats, F. Johansson, F. Pedregosa, M. J. Curry *et al.*, *Peer J. Comput. Sci.* **3**, e103 (2017).
- [42] V. Korobov and V. Ochkov, *Chemical Kinetics with Mathcad and Maple* (Springer, Vienna, 2011).
- [43] G. Vincent, A. Chantre, and D. Bois, *J. Appl. Phys.* **50**, 5484 (1979).
- [44] J. Kerski, P. Lochner, A. Ludwig, A. D. Wieck, A. Kurzmann, A. Lorke, and M. Geller, *Phys. Rev. Appl.* **15**, 024029 (2021).